



Review

Recent advancements in structured-illumination microscopy toward live-cell imaging

Yasuhiro Hirano¹, Atsushi Matsuda^{1,2}, and Yasushi Hiraoka^{1,2,*}

¹Graduate School of Frontier Biosciences, Osaka University, 1-3 Yamadaoka, Suita 565-0871, Japan, and

²Advanced ICT Research Institute Kobe, National Institute of Information and Communications Technology, 588-2 Iwaoka, Iwaoka-cho, Nishi-ku, Kobe 651-2492, Japan

*To whom correspondence should be addressed. E-mail: hiraoka@fbs.osaka-u.ac.jp

Received 3 April 2015; Accepted 8 June 2015

Abstract

Fluorescence microscopy allows us to observe fluorescently labeled molecules in diverse biological processes and organelle structures within living cells. However, the diffraction limit restricts its spatial resolution to about half of its wavelength, limiting the capability of biological observation at the molecular level. Structured-illumination microscopy (SIM), a type of super-resolution microscopy, doubles the spatial resolution in all three dimensions by illuminating the sample with a patterned excitation light, followed by computer reconstruction. SIM uses a relatively low illumination power compared with other methods of super-resolution microscopy and is easily available for multicolor imaging. SIM has great potential for meeting the requirements of live-cell imaging. Recent developments in diverse types of SIM have achieved higher spatial (~50 nm lateral) and temporal (~100 Hz) resolutions. Here, we review recent advancements in SIM and discuss its application in noninvasive live-cell imaging.

Key words: structured-illumination microscopy, super-resolution, temporal resolution, live-cell imaging, low illumination intensity

Introduction

Fluorescence microscopy is a powerful tool for visualizing specific molecules, intracellular structures and biological processes in living cells. However, it has been difficult to observe fine structures within organelles due to the diffraction limit of light, which is ~250 nm (one half of its wavelength) laterally and 500–700 nm axially, formulated by Abbe [1]. In epi-illumination wide-field microscopy, the spatial resolution is easily distorted owing to out-of-focus blur, especially in cases where fluorescent molecules distribute in three dimensions and form fluorescently dense structures, like typical biological samples. Confocal microscopy drastically removes

out-of-focus blur using a pinhole and achieves optical sectioning; however, the spatial resolution is still diffraction limited [2]. Two-photon microscopy uses the two-photon absorption process to excite fluorescent molecules, which occur only at the focus of objective lenses [3] and, thus, provides an optical sectioning effect, but with a diffraction limit similar to confocal microscopy. In stark contrast, during the past two decades, the diffraction limit barrier has been broken by new microscopy techniques termed as super-resolution microscopy, such as stimulated emission depletion (STED) microscopy [4,5], stochastic optical reconstruction microscopy [6], photo-activated localization microscopy [7], super-resolution

optical fluctuation imaging [8], saturated excitation microscopy [9,10] and structured-illumination microscopy (SIM) [11–13] (see reviews [14,15]). In this review, we introduce the basic concept and recent development of one of these techniques, SIM, and discuss its application to biological samples.

The underlying logic of SIM

The use of SIM to obtain super-resolution information simply by illuminating a sample with structured light can be explained in the context of the ‘spatial frequency’ of an image. A fluorescence microscope image reflects the distribution of fluorescent molecules. An enormous number of fluorescent molecules densely localize in a bright structure; neighboring molecules are spatially close, exhibiting high spatial frequency in a dense crowd of molecules. However, high-frequency information is lost after light passes through an objective lens. If a microscope can collect high spatial frequency information, closely spaced molecules can be resolved from each other; however, if a microscope collects only low spatial frequency information, then such molecules cannot be resolved (Fig. 1a, real space). Accordingly, high-resolution objects in real space have high spatial frequencies in reciprocal (frequency) space, and low-resolution objects have low spatial frequencies (Fig. 1b, comparison between real space and reciprocal space). Information for both real and reciprocal spaces can be converted to each other using the Fourier transform (FT) or inverse FT. Abbe’s diffraction limit, which is defined by the numerical aperture (NA) of the objective lens and the wavelength of light, determines the maximum spatial frequency (also termed the cutoff frequency) and is drawn as a circle in two dimensions (2D) and a pancake-like shape in three dimensions (3D) in reciprocal space. Therefore, a microscope can only collect information within the circle referred to here as the ‘observable region’ in reciprocal space, which corresponds to the ‘resolution’ in real space. The observable region can be determined by the area covered by the optical transfer function (OTF), i.e. the FT of the point-spread function (PSF). ‘Super-resolution’ refers to the ability to acquire information outside of the observable region in reciprocal space. To achieve this, SIM uses a moiré effect generated by illuminating the sample with structured light (Fig. 1b). When two periodic patterns are superimposed, a coarser pattern termed a moiré fringe appears (Fig. 1b, real space). This can be illustrated by the generation of new spatial frequency of the object shifted exactly by the frequency of the structured pattern (Fig. 1b, blue clouds in reciprocal space). Because of this effect, high-frequency information that is normally unresolvable using conventional microscopy moves into the observable region (Fig. 1b, blue clouds in the orange circle). The high-frequency

information can be reconstructed by computation using the information resolvable with conventional microscopy.

The basic SIM procedure

The SIM design is based on wide-field microscopy, as reported by Gustafsson [12] and has been applied to biological samples [16–18]. SIM mainly consists of two key parts: (i) sample illumination by a periodic pattern and (ii) computational reconstruction of a super-resolution image.

In the initial SIM setup (Fig. 2a), light is divided by diffraction grating. The ± 1 st-order diffracted beams for 2D-SIM [12] or the 0th- and ± 1 st-order beams for 3D-SIM [13] are assembled at the sample plane and interfere with each other to produce a sinusoidal illumination pattern. Three or five lateral frequency components ($m = 0, \pm 1, \pm 2$), corresponding to the FT of the sinusoidal illumination pattern, appear in reciprocal space in 2D- or 3D-SIM, respectively (Fig. 2b). The direction and distance from the origin (direction vector; \mathbf{p}_m) reflect the direction and line spacing of the illumination pattern, respectively. The raw data obtained by 3D-SIM is the sum of five elements of information derived from different lateral frequency components that contain unresolvable information under a diffraction-limited microscope (Fig. 2b, raw data in real space and top panel in reciprocal space. See also Fig. 1b).

To separate the information, a set of five images with illumination phases shifted by steps of $2\pi/5$ was used. After separation, the offset position (distance from the origin $|\mathbf{p}_m|$) and the amplitude of the illumination pattern were determined for each set of super-resolution information (‘separation’ and ‘ \mathbf{p}_m and amplitude determination’ in Fig. 2b). Each component was deconvolved using a Wiener filter to generate a uniform information distribution in reciprocal space (‘Wiener filter’ in Fig. 2b). Finally, each component was moved to the correct position and merged based on the offset and amplitude of the illumination pattern determined above (‘shifting’ and ‘merging’ in Fig. 2b). Thus, the total OTF was extended (in distance and direction) in a manner that depends on the frequency components. Importantly, since the illumination pattern was generated using an objective lens, the distance from the origin ($|\mathbf{p}_m|$, equal to the fineness of line spacing in real space) is diffraction limited. Therefore, the resolution for this setup is improved by a factor of two.

To increase the resolution isotopically, the pattern was rotated two or more times (‘merging 3-angles’ and ‘reconstructed 3D-SIM image’ in Fig. 2b). In 3D-SIM, the sinusoidal pattern was generated in both the lateral and axial directions, resulting in resolution improvement in three dimensions (Fig. 2c and d). See references [13,19] for a

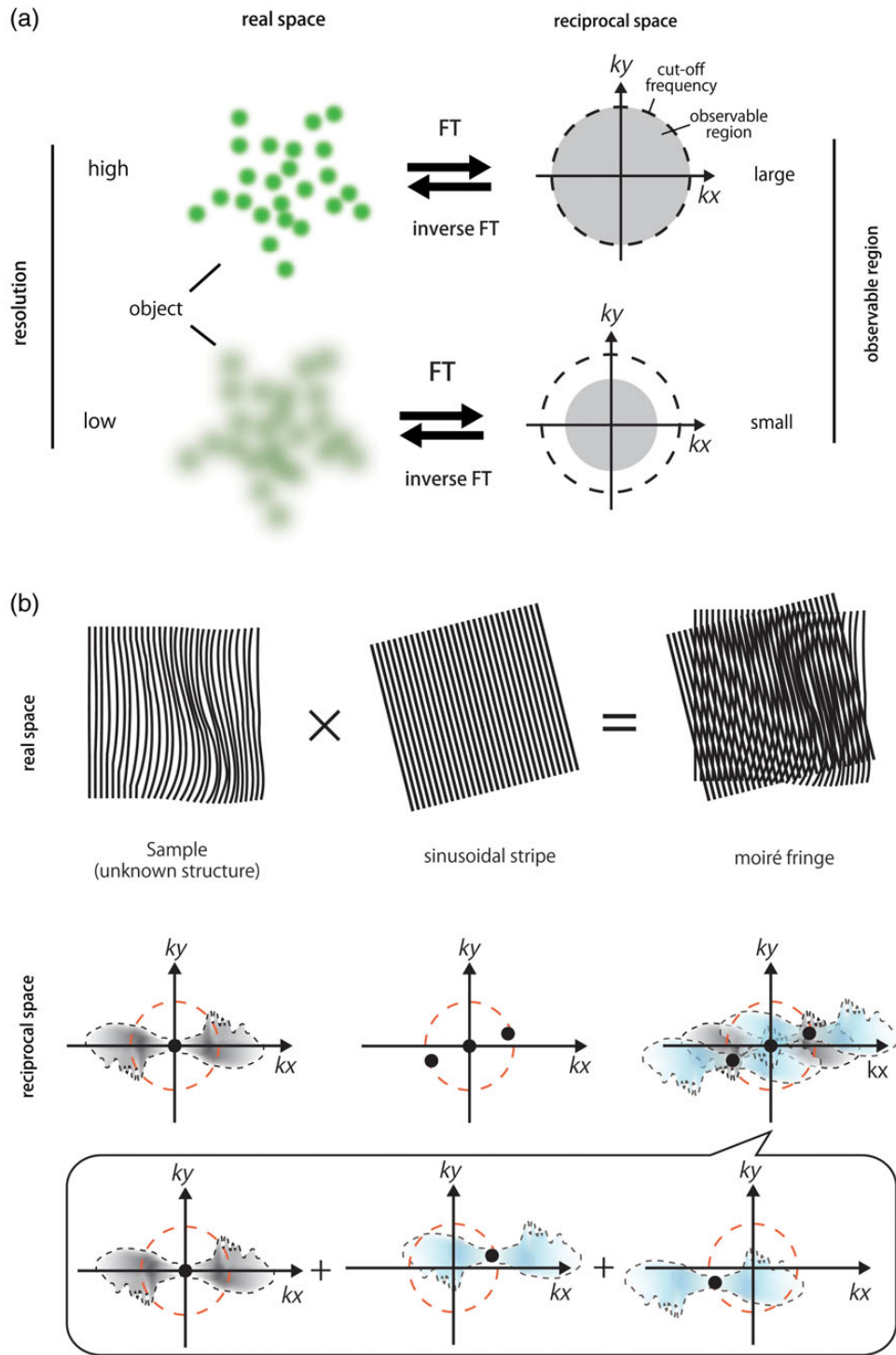


Fig. 1. The underlying logic of SIM. (a) Relationship between real and reciprocal spaces. A representation of image information is reciprocal and transformed back and forth by FT or inverse FT. Gray and dashed circles indicate spatial frequency (k) of an object in the lateral direction and a diffraction limit, respectively. (b) Moiré effect. If two periodic patterns interfere with each other, a coarser pattern (moiré fringe) appears. Using this coarse image, information beyond the resolution limit can be collected by conventional microscopy. Top and bottom panels indicate real and reciprocal space, respectively. In the bottom panels, dashed orange circles indicate spatial frequency of the diffraction limit. Gray and blue clouds indicate spatial frequency of an object and spatial frequency generated by the moiré effect, respectively. Black dots indicate frequency components of the illumination pattern. The generation of blue clouds moves unobservable information from the gray cloud outside the orange circle into the observable orange circle.

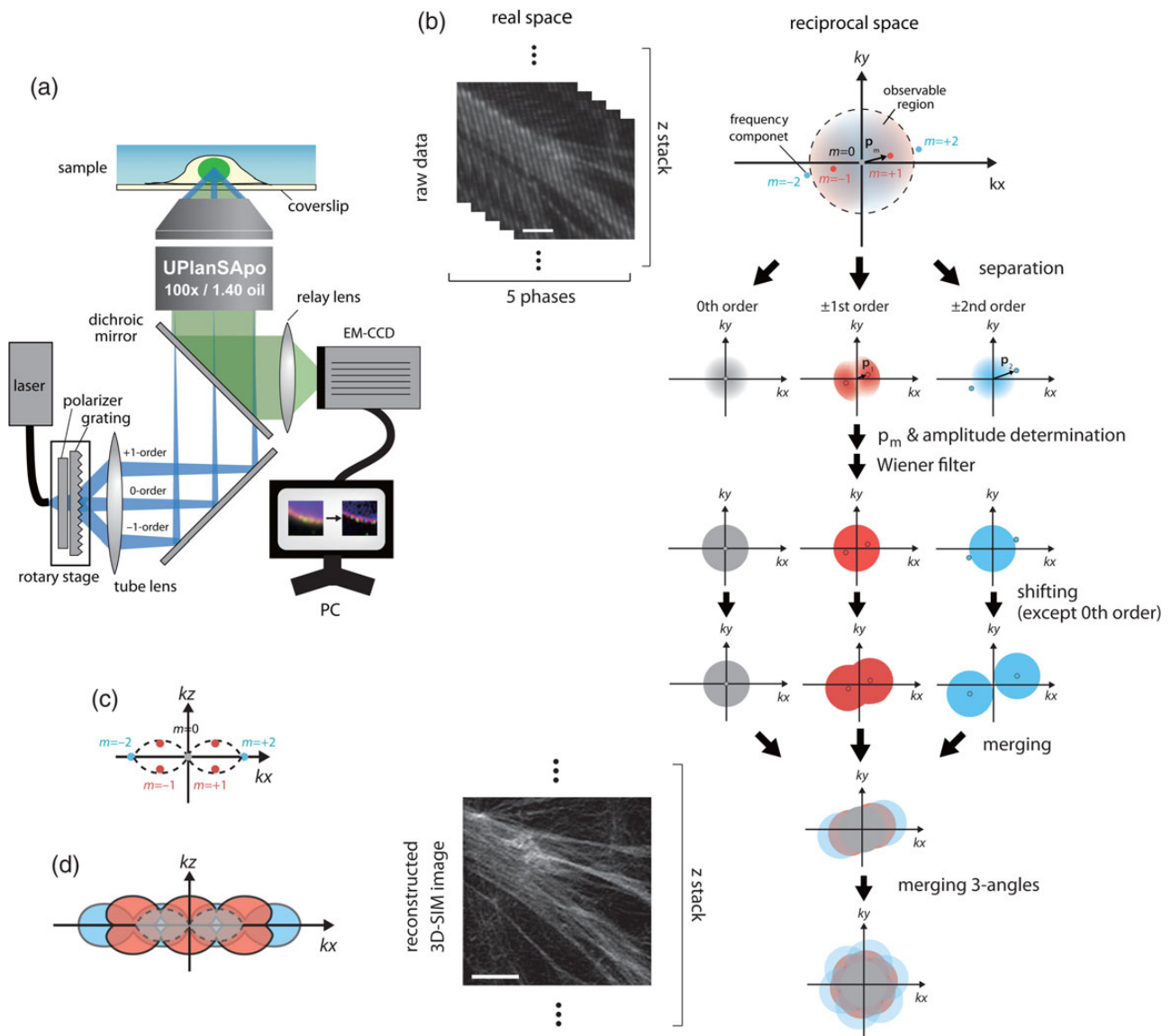


Fig. 2. The basic SIM procedure. (a) Simplified optical setup of 3D-SIM. Polarized light is separated by grating. Zero- and ± 1 -order diffraction light are focused on the back focal plane of the high NA objective lens to generate a sinusoidal pattern. The grating is held on a piezoelectrically driven stage to move the phase of illumination light and is mechanically rotated to change the angle of the stripe pattern. Images containing super-resolution information are recorded by a camera. Finally, a super-resolution image is reconstructed by computational methods. (b) The reconstruction process of the super-resolution image. Raw data obtained by 3D-SIM contain five different pieces of information derived from different frequency points (raw data in real space, and top panel in reciprocal space). Five phase-shifted images were taken, and the information was then separated. After the offset (p_m) and amplitude of the illumination pattern were determined, the information was filtered by a Wiener filter. Finally, the information was moved to the correct position. This process was repeated in two more directions, and then the super-resolution image was obtained (reconstructed 3D-SIM image). Bars; 1 μm . (c and d) Axial resolution enhancement of 3D-SIM. A sinusoidal pattern was formed not only in the lateral but also in the axial direction (c). Hence, the total OTF was expanded in the axial direction (d).

detailed description of SIM theory and the reconstruction process.

The concept of SIM, i.e. illumination with a pattern followed by computational calculation, can be easily combined with other types of light microscopy owing to its simple theoretical basis. Indeed, combinations of SIM with confocal, two-photon, total internal reflection fluorescence, surface plasmon [20,21] and coherent anti-Stokes Raman scattering [22] microscopies have successfully increased resolution.

Merits and demerits of SIM

SIM has two major advantages over other super-resolution techniques. First, axial resolution doubling in 3D-SIM greatly reduces out-of-focus fluorescence and plays an important role in improving signal-to-noise ratio (SNR). Thus, SIM is capable of achieving an optical sectioning effect. Second, common fluorophores can be used with no special properties required and is suitable for multicolor imaging.

In contrast, there are three disadvantages. First, the resolution enhancement (a factor of two) is less than that of other super-resolution techniques. Second, SIM (as in most other super-resolution techniques) requires the acquisition of many image frames to reconstruct one super-resolution image. This results in low temporal resolution and often photobleaching, even though the illumination intensity is 10^2 – 10^3 times lower than that of confocal-based super-resolution microscopy, such as STED. Third, SIM (again, as in most other super-resolution techniques) is sensitive to spherical aberration. The illumination patterns are degraded in the presence of spherical aberration, reducing the amount of information in higher frequency. Consequently, it becomes difficult to observe regions far from the coverslip if a spherical aberration is introduced by refractive-index mismatch among glass, lens-immersion medium and a biological sample. However, some of these disadvantages have been overcome by recent technological advances in SIM. Those properties are summarized in Table 1.

Resolution enhancement beyond a factor of two

The resolution of SIM is linearly proportional to the frequency of the sinusoidal pattern or the pitch of lines of structured excitation light, but the resolution improvement is limited by the diffraction limit of excitation light as described above (see ‘The basic SIM procedure’). This resolution limit has been overcome by breaking the sinusoidal pattern into more complex patterns using nonlinear optics [25]. Under a low illumination power density below the saturation level, a fluorophore is excited and emits fluorescence linearly. In contrast, under a high power density, the excitation rate exceeds the decay rate resulting in a nonlinear response. Under this condition, the expected fluorescence response is no longer sinusoidal, but trapezoidal, which contains a series of higher-order harmonics of a sinusoidal wave (Fig. 3a, saturated structured-illumination microscopy (SSIM)). Since these higher-order harmonics contain information beyond the observable region in reciprocal space, the resolution can be enhanced by more than a factor of two by the analogy of linear SIM (Fig. 3b and c). Therefore, there is no longer a theoretical resolution limit by using infinite harmonics. Gustafsson reported that SSIM based on 2D-SIM can achieve <50-nm resolution [25]: illuminating 50-nm diameter fluorescent beads at 5.3 mJ cm^{-2} ($\sim 9 \text{ MW cm}^{-2}$), 9-phase \times 12-rotation (total 108) images were obtained and then the first three harmonics were used to reconstruct a single super-resolution image. The average full width of half maximum (FWHM) of the beads was $58.6 \pm 0.5 \text{ nm}$ (after removing the size effect of the bead, it was $48.8 \pm 0.5 \text{ nm}$), which was 5.5 times greater than that

of conventional microscopy (265 nm). Despite the spatial resolution enhancement, SSIM suffers two major drawbacks. Although the illumination power used in SSIM is more than three orders of magnitude lower than that in two-photon microscopy, the high power density induces severe photobleaching. In addition, the temporal resolution is low, since SSIM needs more images than SIM to reconstruct super-resolution images and relatively long exposure time per frame (0.15 s) to obtain enough SNR of higher-order harmonics. For these reasons, using SSIM for biological samples is difficult.

The illumination intensity problem of SSIM may be lowered by several orders of magnitude using the photo-switchable fluorescent protein Dronpa [33–35]. Dronpa has major and minor excitation peaks at 503 and 390 nm, respectively, and an emission peak at 518 nm [33]. When excited by blue light (i.e. 488 nm), Dronpa emits fluorescence and transitions to its ‘off’ state. Dronpa reverts back to its ‘on’ state when illuminated by UV light (i.e. 405 nm). This cycle can be observed over 100 times, though the fluorescence intensity gradually decreases ($\sim 75\%$). The transition from the ‘off’ to ‘on’ state occurs immediately at a very low illumination power ($\sim 0.1 \text{ W cm}^{-2}$). Thus, Dronpa has attracted researchers’ attention as a fluorescent source for nonlinear response under low illumination conditions [36]. Rego *et al.* [26] used Dronpa to generate finer illumination stripes than the diffraction limit by saturating the ‘off’ state at low illumination intensity (1 – 10 W cm^{-2}) (Fig. 3a, NL-SIM (Dronpa)). Using Dronpa, they observed purified microtubules, nuclear pore complex components and actin fibers in the fixed cells using 5 W cm^{-2} of a 488-nm laser for saturation and obtained a FWHM of $\sim 50 \text{ nm}$ with first- and/or second-order harmonics. In this method, photoswitchable proteins are required to repeat photon emission over 50 times (depending on the desired resolution) without decreasing the number of photons per cycle. The exciting point of this method is that the nonlinear phenomenon is achieved at quite low illumination intensity, indicating the possibility for live-cell imaging at resolutions of <50 nm.

SIM described above can enhance resolution by 2-fold or more. However, the axial resolution is about three times lower than the lateral resolution, even in 3D-SIM. Shao *et al.* [37] reported a new microscope system, I³S microscopy, in which two objective lenses illuminate the sample, similar to 3D-SIM but from both sides. Thus, six beams (three from one objective and three from the other) interfere pairwise, and the resulting 19 different frequency components distribute equally in three dimensions. Therefore, an isotropic super-resolution image can be reconstructed, providing a spatial resolution of <100 nm in all three dimensions [37].

Collectively, the resolution of SIM is unlimited if the sinusoidal pattern is broken and can be isotropic using I³S.

Table 1. Comparison of SIM performance

	2D-SIM	3D-SIM	SSIM	NL-SIM (Dronpa)	ISM	MSIM	CSD-ISM	Instant SIM	Bessel SIM	Lattice SIM
Spatial resolution (nm)										
X	~100	~120	~50	~50	~150	~145	~145	~145	~180	~150
Y	~100	~120	~50	~50	~150	~145	~145	~145	~230	ND
Z	ND	~360	ND	ND	ND	~400	~350	~350	~350	~280
Illumination pattern	Sinusoidal strip (TIRF)	Sinusoidal strip	Sinusoidal strip (2D)	Sinusoidal strip (TIRF)	Point	Multifocus	Multifocus	Multifocus	Parallel Bessel beam	Hexagonal lattice
Pattern generation device	SLM	SLM	Grating	Grating	Laser spot	DMD	CSD	CSD	Grating	SLM
NA of objective lens used	1.49	1.2	1.4	1.46	1.2	1.45	1.49	1.45	0.3–0.65 (EL), 0.8– 1.1 (DO)	0.48–0.55 (EL), 1.1 (DO)
Excitation wave length (nm)	488	488	532	488	640	488, 561	400, 488, 561, 647	488, 561	488, 561	488
Field of view ($\mu\text{m} \times \mu\text{m}$)	8 × 8	>20 × 20	>25 × 25	>50 × 50	2 × 2	48 × 49	ND	>70 × 50	>50 × 50	36.8 × 36.8
Frame rate (2D, Hz)	11	3.6 (0.2 Hz/ volume)	~0.06	~0.01	0.04 ^a	~1	~1	~100	10–20	~50
Illumination intensity (W cm^{-2})	~5–10	~5	~9 × 10 ^{6a}	~1–10	~1.5 × 10 ^{3a}	~10 ¹ –10 ^{2a}	ND	~5–50	ND	93 μW (total power)
Reference	[23]	[24]	[25]	[26]	[27]	[28]	[29]	[30]	[31]	[32]

ND, not described; TIRF, total internal reflection fluorescence.

^aCalculated from their description.

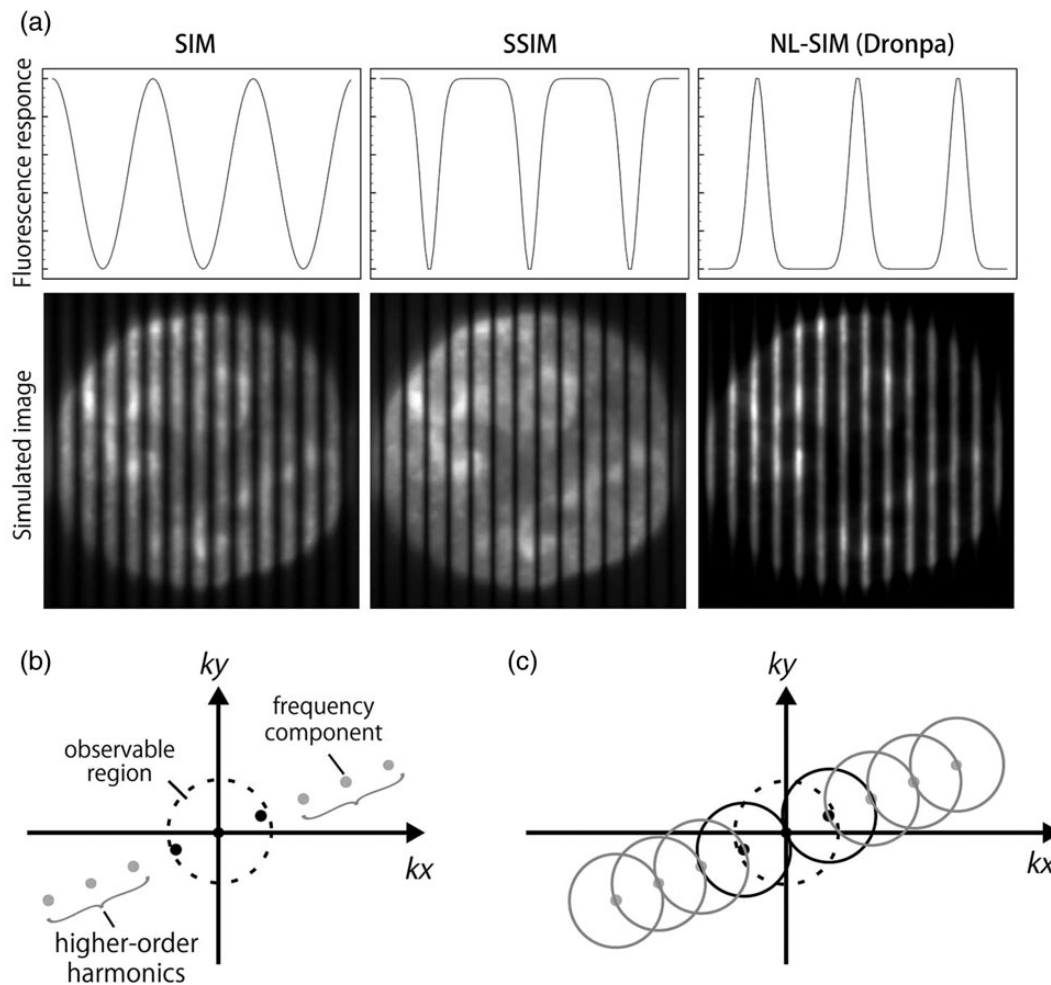


Fig. 3. Resolution enhancement beyond a factor of two. (a) Pattern generation finer than the diffraction limit. When illumination intensity is increased beyond a certain point, the fluorescence response cannot increase linearly (saturation). Therefore, the space between fluorescence peaks decreases (SSIM). By using the photoswitchable protein Dronpa, the same but inverted pattern can be generated (NL-SIM (Dronpa)). If the blue light that forces Dronpa in its 'off' state is saturated, Dronpa emits fluorescence only from narrow regions. A fluorescence image of the cell nucleus superimposed on the simulated, but low-frequency, patterns is shown below each plot to help understanding the fluorescence response. The finer illumination pattern results in frequency points outside of the observable region (b), and then the resolution is improved beyond a factor of two (c). Black and gray dots in (b) and (c) indicate frequency points from a linear and nonlinear response, respectively.

Although combining these two methods is extremely attractive, both methods are still too demanding for conventional biological imaging. It is especially difficult to satisfy the theoretical assumption of NL-SIM, namely that fluorophores emit an infinite number of photons. Further improvement of photoswitchable fluorophores is strongly desired.

New directions for improving temporal resolution

Because SIM requires many raw images to reconstruct a single super-resolution image, the temporal resolution is inevitably too low to observe objects in living cells. The distance that objects travel during data acquisition must be

shorter than the spatial resolution (i.e. $\sim 100 \text{ nm s}^{-1}$) to avoid motion artifacts during reconstruction.

In the original optical design of SIM, the phase and angle of the illumination pattern move mechanically. Those motions, especially rotation, are too slow, such that it takes $\sim 10 \text{ s}$ to obtain only a few micrometer z-stacks. To improve this, a ferroelectric liquid crystal spatial light modulator (FLC-SLM) is used to replace the diffraction grating [23,24]. It is possible to control the wavefront of input light by changing the liquid crystal alignment; thus, the desired illumination pattern can be generated in $< 1 \text{ ms}$ owing to the short response time of FLC-SLM, greatly improving the temporal resolution of SIM compared with that of a motor-based system. By using FLC-SLM and custom FLC phase retarders,

Kner *et al.* [23] and Shao *et al.* [24] have achieved ~ 100 nm resolution at frame rates of 11 and 0.2 Hz in 2D- and 3D-SIM, respectively (although it depends on the imaging size and thickness of the samples). The only remaining limiting factors for temporal resolution are the exposure time, determined by the brightness of samples, and readout rate of the camera. For further improvement of temporal resolution, recently developed scientific complementary metal oxide semiconductor cameras, which realize faster readout, could possibly substitute frame-transfer electron-multiplying charge-coupled device (EM-CCD) cameras, although EM-CCD still has the advantage of obtaining high SNR of extremely dark samples.

Image scanning microscopy: SIM with point-scan illumination

Improvement of the temporal resolution has also been attempted by different approaches. Structured patterns of illumination to obtain the super-resolution information in SIM are not limited to the sinusoidal pattern described above. Recent methods in super-resolution microscopy, classified as SIM, realize high temporal resolution using alternative illumination patterns. Multifocal structured-illumination microscopy (MSIM) [28], confocal spinning-disk image scanning microscopy (CSD-ISM) [29] and instantaneous SIM (instant SIM) [30] obtain super-resolution information using a multifocal illumination pattern. These methods are based on ISM, reported by Müller and Enderlein [27] (Fig. 4).

ISM is essentially a type of point-scanning confocal microscopy; however, the fluorescence that passes through the pinhole is recorded by a multipixel camera, unlike conventional confocal microscopy, which uses a photomultiplier tube (Fig. 4a, compare ISM with confocal microscopy). The concept of ISM is similar to that of SIM. In other words, ISM is a special type of SIM. The illumination of ISM is a tightly focused laser spot, equivalent to a single period of the sinusoidal stripe used for illumination in SIM (Fig. 4a, arrowhead). Although increased resolution of SIM is limited along the pattern direction, that of ISM is isotropic.

To understand why the resolution of ISM is improved by using a multipixel camera, we examined how the PSF is formed in confocal microscopy and the roles of camera pixels in ISM. Effective PSF (PSF_{eff}) in confocal microscopy is a product of two PSFs: PSF made by illumination (PSF_{illu}) and PSF made by emission that passes through the pinhole (PSF_{emPH}). If the illumination beam, pinhole and detector (photomultiplier tube) in confocal microscopy are coaligned with the optical axis, PSF_{illu} completely overlaps with PSF_{emPH} ($d = 0$ in Fig. 4b). Thus, the PSF_{eff} becomes sharper, theoretically supporting a lateral resolution that is $\sqrt{2}$ times higher if the pinhole is infinitely small [2]. When the pinhole

is displaced by a certain distance d from the optical axis, PSF_{emPH} is also shifted by d in the same direction. As a result, PSF_{eff} is moved by approximately $d/2$ in the same direction and its peak intensity decreases ($d = 1.5$ and 3 a.u. in Fig. 4b). Remarkably, the PSF_{eff} formed by the displaced pinhole is sharper than the nondisplaced PSF, and its effect is a function of d (Fig. 4c).

In ISM, a blurred spot distributed over camera pixels is obtained as a raw image. Under the condition that the illumination beam and pinhole are aligned, the pixel corresponding to the peak of the blurred spot (the black dot in 'ISM' in Fig. 4a) is on the optical axis. Therefore, information obtained from the pixel equals the information obtained from confocal microscopy. In contrast, the information detected at d from the optical axis is equivalent to the information passing through the pinhole displaced by d . Thus, the PSF_{eff} should be formed at $d/2$ from the center. To reconstruct the PSF of ISM, all information is moved back by $-d/2$ and summed; in other words, the blurred spot is shrunk by a factor of two. By repeating this process for each illumination position, an ISM image is constructed.

ISM has a significant advantage with respect to the SNR in obtaining super-resolution information compared with confocal microscopy. Improving the resolution of confocal microscopy by closing the pinhole is not practical because almost all photons are rejected. In contrast, ISM obtains super-resolution information using camera pixels as small pinholes without rejecting photons and shifts the distributed photons back. The resolution of ISM, however, is lower than that of SIM because ISM uses a single illumination spot to obtain super-resolution information, while SIM uses a combination of multiple lines to create moiré, which makes super-resolution information accessible (Fig. 1b).

In practice, to reconstruct a super-resolution image, the geometric relationship between the coordinate of the illumination spot and the coordinate of detection of the corresponding spot on camera is precisely calibrated at first. After this, a portion of raw images at the detection spot are shrunk by a factor of two and mapped in the coordinate of illumination, or raw images are mapped in the $\times 2$ -magnified illumination coordinate (Fig. 4b). This process is repeated for all images taken at different illumination positions. If raw images are summed without shifting, it coincides with a conventional confocal image. Finally, high-resolution information of ISM is enhanced by deconvolution using a Wiener filter, just like SIM reconstruction (Fig. 2). By using deconvolved ISM, FWHM of 100-nm diameter fluorescent beads became 1.63 ± 0.08 times smaller (150 ± 10 nm) than that of conventional confocal microscopy (244 ± 9 nm) [27]. Axial resolution of ISM is determined by the pinhole size, similar to conventional confocal microscopy; thus, ISM inherits the intrinsic optical sectioning capability of

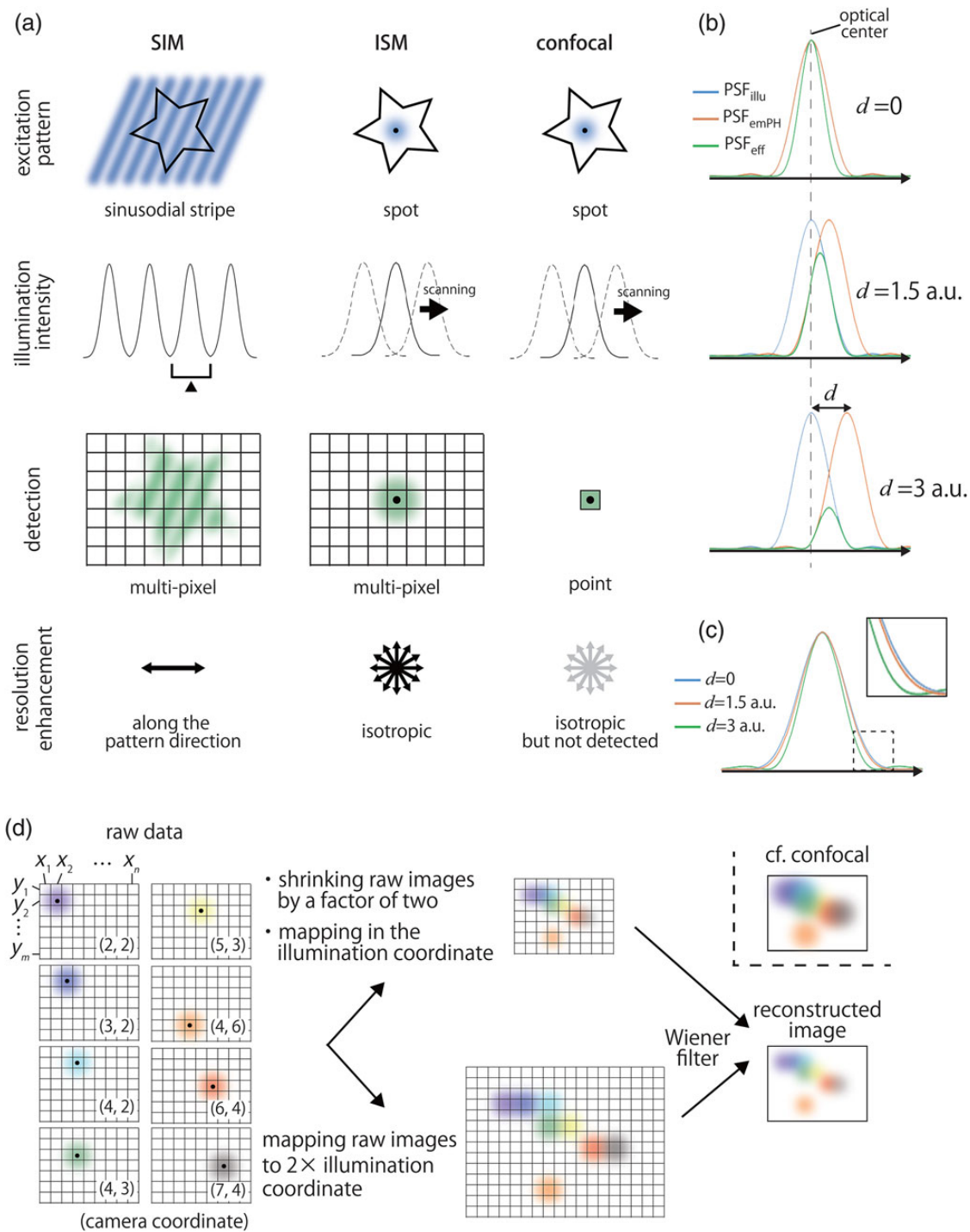


Fig. 4. Concept of ISM family. (a) ISM setup. ISM uses a tightly focused laser spot, to excite the fluorophore, and a multipixel-based camera, instead of a photomultiplier tube, for detection. Although the illumination of ISM is a spot, it is equivalent to one period of sinusoidal stripe used in SIM (arrowhead). Although resolution enhancement of SIM is limited along the pattern direction, the resolution enhancement of ISM is isotropic. Conventional confocal microscopy also has this effect, but cannot be obtained due to point detection. (b, c) Resolution enhancement of ISM. (b) Effect of pinhole displacement. If the illumination beam and pinhole are aligned, the illumination PSF (PSF_{illu}) and the detection PSF (PSF_{emPH}) completely overlap (if Stokes's shift is ignored). In this situation, the PSF_{eff} corresponds to the confocal PSF (top). When the pinhole is displaced by a certain distance d , the PSF_{eff} shifts to $d/2$, becomes sharper and the amplitude of the peak decreases depending on d (middle and bottom). a.u. represents arbitrary units. (c) Three PSF_{eff} formed at different d values are centered and normalized. The dashed square region is enlarged at the top right. (d) Reconstruction process. Raw data of ISM are a blurred image. The geometric relationship between the coordinate of the illumination spot and the coordinate of detection of the corresponding spot on camera is precisely calibrated. Raw images are either shrunk by a factor of two and mapped in the illumination coordinate (upper) or mapped in a $\times 2$ -magnified illumination coordinate (bottom). If raw images are summed, it coincides with a conventional confocal image.

confocal microscopy. Since ISM itself is basically point scanning and requires high pixel density to satisfy Nyquist's sampling theory, poor temporal resolution (25 s for $2\ \mu\text{m} \times 2\ \mu\text{m}$) is obtained.

Fast ISM

MSIM [28] and CSD-ISM [29] use multifocal excitation generated by a digital micromirror device (DMD) and CSD, respectively. MSIM uses an approximately equilateral triangular lattice of spots as an illumination pattern. After taking raw images (224 images for one MSIM image), digital pinholing by an appropriate Gaussian mask to each spot, $2\times$ scaling, summing and deconvolution, they obtained $\sim 145\text{-nm}$ lateral and $\sim 400\text{-nm}$ axial resolution with $\sim 1\ \text{Hz}$ 2D frame ($45.6\ \mu\text{m} \times 45.6\ \mu\text{m}$) rate. On the other hand, CSD-ISM used a commercially available CSD, which comprised two arrays, a microlens array and coaligned pinholes, to generate a multifocal excitation pattern. Schulz *et al.* imaged 85 z-stacks ($17\text{-}\mu\text{m}$ thickness) of GFP-3PO-Tau aggregates with $\sim 1\ \text{Hz}$ 2D frame rate ($\sim 0.8\ \text{s}$ per frame) with a similar resolution enhancement effect (a factor of $\sim 1.35\text{--}1.55$). Instant SIM uses CSD similar to CSD-ISM and implements most reconstruction steps with hardware by adding a second microlens array coaligned with the first microlens array and pinholes [30]. The second microlens array shrinks the pinholed image by a factor of two and, thus, the obtained image is already rescaled without computational calculation. By sweeping the multifocal illumination pattern by a galvanometric mirror during a single exposure of the camera, the rescaled images are summed, and then a super-resolution image is produced. This method combined with deconvolution allowed up to a 100-Hz frame rate with 145-nm lateral and 350-nm axial resolution.

Although the spatial resolution is lower than that of SIM, ISMs have great potential for multicolor live-cell

imaging. Because ISM-based microscopy is (i) applicable for multicolor imaging and nonlinear optics, like SIM [38,39], and (ii) more tolerant to a spherical aberration than SIM because it does not need to modulate illumination patterns. In particular, instant SIM is beneficial for live-cell imaging owing to its high temporal resolution.

SIM based on light-sheet illumination

Another interesting approach is light-sheet microscopy using a plane illumination [40,41]. A thin light sheet is generated by a cylindrical lens and/or an objective lens that acts as an excitation lens (EL) to excite the fluorophore, and then the emitted fluorescence is detected by an objective lens set perpendicularly along the illumination plane (detection objective lens: DO). The plane illumination is equivalent to optical sectioning, but advantageous for reducing out-of-focus fluorescence compared with epi-illumination wide-field microscopy, although the thickness of the illumination plane depends on the NA of EL. Furthermore, it exhibits a higher temporal resolution than conventional confocal microscopy. A sample is illuminated from its side, so this method is applicable for thick samples, such as multicellular organisms. Betzig and colleagues [31,42] used a periodic illumination pattern in Bessel beam plane illumination (Fig. 5a). A Bessel beam can be created by projecting an annular illumination at the back focal plane of the EL, resulting in a self-reconstructing light beam. Therefore, this beam is less sensitive to scattering in the sample compared with a Gaussian beam [43,44]. The authors generated parallel Bessel beams by a Dammann grating-based diffractive optical element as structured illumination, obtained N phase-shifted images (the number of required raw data depends on how many frequency components should be separated) and reconstructed a super-resolution image by the analogy of SIM (Bessel SIM). Because the illumination pattern is formed only along the

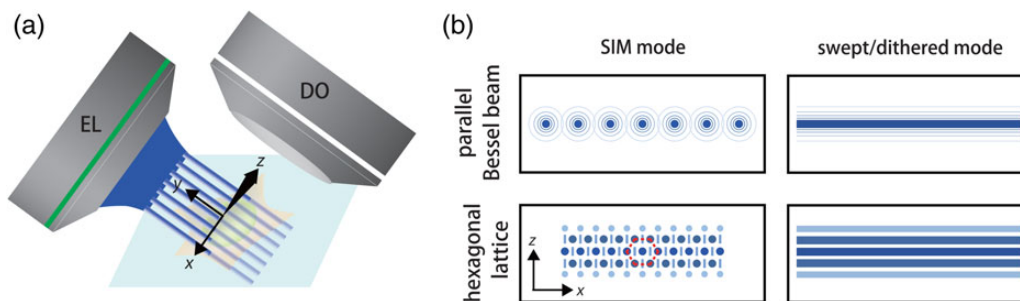


Fig. 5. SIM using a Bessel beam. (a) Setup of Bessel SIM. A sample is illuminated with seven parallel Bessel beams separated by grating from an EL. The illumination pattern is swept along the x direction to change the phase. Fluorescence is detected by the DO, which is located vertically. (b) Schematic illustration of illumination patterns at the xz plane of Bessel SIM and lattice SIM. Those methods use parallel Bessel beams and a hexagonal lattice for illumination light. In the swept/dithered mode, those patterns are swept along the x direction during the camera exposure time and, thus, the time-averaged uniform pattern is generated. Red dashed hexagon indicates one period.

direction orthogonal to illumination, resolution enhancement is obtained only in this direction (Fig. 5b, top panels). Bessel SIM achieved 10–20 Hz frame rates with 180 nm \times 230 nm \times 350 nm resolution in the x -, y - and z -axis, respectively.

Another illumination pattern of a hexagonal lattice, periodic in both the lateral and axial axes using SLM (lattice SIM), was used by Chen *et al.* [32] (Fig. 5b, bottom panels). Lattice SIM achieved 150- and 280-nm resolution in the x - and z -axis, respectively, at \sim 50-Hz frame rate. The authors reported another swept/dithered mode of lattice SIM, in that the time-averaged uniform illumination across the xy plane is made by sweeping the hexagonal lattice pattern in the x direction during the camera exposure time (Fig. 5b, bottom right). In this mode, although the resolution is diffraction limited, each illumination plane is tightly focused and has low background, resulting in resolution enhancement in the z direction. Finally, the swept/dithered mode of lattice SIM achieved up to a 100-Hz frame rate with 230-nm lateral and \sim 370-nm axial resolution.

Toward visualization of a cell in living color

Recent advances in the family of SIM have opened the door for real-time super-resolution imaging to more precisely understand biological processes in living cells. However, gaps between technology and biology still need to be filled.

First, the aberration of light must be corrected. Aberration of light, especially a spherical aberration derived from samples, leads to the following: (i) on the excitation side, reduction of the SNR (amplitude) of the illumination pattern results in reduction of super-resolution information, and (ii) on the emission side, deformation of PSF results in a loss of photon and an artifact during reconstruction [45]. Thus, aberration-less imaging is quite important for filling this gap. A silicone-immersion objective lens uses an immersion oil with a refractive index ($n = 1.404$) close to the refractive index of a cell ($n \approx 1.38$) and has a higher NA (1.30 or 1.35) than a water-immersion lens (NA \approx 1.1–1.2); thus, this lens is expected to improve the image quality of SIM deeper inside live cells than oil-immersion objective lenses. However, an objective lens alone cannot correct local refractive-index mismatch, such as borders between the organelle and the cytoplasm or cell–cell connection. Adaptive optics (AO), originally developed for astronomy telescopes to cancel the Earth's atmospheric turbulence [46], can be implemented for microscopy. AO aims to correct aberrations of light by reducing wavefront distortions. The distortion of a wavefront is measured by a wavefront sensor at the pupil plane and is corrected by an active optical element, such as a deformable mirror or SLM, to recover ideal performance. Several groups have used AO for biological samples [47,48]. Wang *et al.* [49] obtained a near

diffraction-limited fluorescent signal emitted from a depth of >200 μ m from a living zebrafish brain. AO is expected to work in super-resolution imaging, improve the resolution and SNR and extend the depth of observation farther away from the coverslip surface. With these approaches, sample-induced aberrations may be canceled to improve the quality of SIM reconstruction.

Second, phototoxicity during imaging must be reduced. Acquiring high SNR always results in a trade-off between illumination intensity and phototoxicity. If we can increase the illumination density infinitely and, if the excited fluorophore can emit photons infinitely without photobleaching, we will be able to obtain almost infinite spatiotemporal resolution. In practice, however, the illumination intensity should be kept as low as possible so that the illumination does not affect biological processes. Unfortunately, current methods of SIM reconstruction have limited the capability of separating high-resolution information from noise and, as a result, noise tends to be enhanced during the filtering process of low SNR images taken under low illumination conditions. Improvements in optical elements, brighter and more photostable gene-encoded fluorescent probes and cameras with high quantum yield and low noise are strongly desired. On the software side, noise reduction before or during reconstruction of SIM is important for minimizing artifacts and improving both resolution and SNR. We found that denoising [50] and entropy-regularized deconvolution (ER-Decon) [51] are quite valuable and may be used for SIM reconstruction. Denoising is a patch-based noise-filtering algorithm that allows recovery of the signal from low SNR images by minimizing Poisson–Gaussian noise [52], and as a result, high SNR images can be obtained under the illumination intensity reduced by approximately three orders of magnitude [53]. ER-Decon is a new deconvolution algorithm based on the total variation (TV) method and can recover object information from an image that is almost indistinguishable from noise. It allows the reduction of illumination intensity by two orders of magnitude. The TV method [54–57] is also applicable to SIM reconstruction processing. Chu *et al.* [54] applied a TV constraint instead of a Wiener filter and obtained a similar reconstructed image quality, even with two orders of magnitude lower illumination intensity, without sacrificing the resolution of SIM (\sim 110 nm lateral and \sim 300 nm axial resolution from 100-nm diameter fluorescent bead observation).

These new approaches will promote live-cell imaging with a high spatiotemporal resolution under low illumination intensity.

Conclusion

In the last decade, the spatiotemporal resolution of SIM has been greatly improved by exploiting state-of-the-art optics

and by implementing alternative illumination methods. Surprisingly, the illumination pattern of SIM no longer needs to be a known pattern. Mudry *et al.* [58] reported that super-resolution information can be made available by illuminating a sample with several uncontrolled random speckles, without sacrificing resolution. This suggests that optimization of illumination patterns might allow for a reduction in the number of raw data required to reconstruct SIM images and, thus, increase temporal resolution and reduce photo-damage to cells. By combining the techniques summarized here, non-invasive, high-rate live-cell imaging can be achieved with <100-nm spatial resolution in future studies.

Acknowledgements

We thank Tokuko Haraguchi for developing live-cell imaging microscopy and insightful discussion during this study.

Funding

This work was supported by Ministry of Education, Culture, Sports, Science, and Technology, Japan, KAKENHI (25840008 to Y. Hirano, 26292169 to A.M. and 26251037 and 26116511 to Y. Hiraoka).

References

1. Abbe E (1873) Beiträge zur Theorie des Mikroskops und der mikroskopischen Wahrnehmung. *Arkiv. Mikroskop. Anat.* 9: 413–468.
2. Sandison D R, Piston D W, Williams R M, Webb W W (1995) Quantitative comparison of background rejection, signal-to-noise ratio, and resolution in confocal and full-field laser scanning microscopes. *Appl. Opt.* 34: 3576–3588.
3. Denk W, Strickler J H, Webb W W (1990) Two-photon laser scanning fluorescence microscopy. *Science* 248: 73–76.
4. Hell S W, Wichmann J (1994) Breaking the diffraction resolution limit by stimulated emission: stimulated-emission-depletion fluorescence microscopy. *Opt. Lett.* 19: 780–782.
5. Klar T A, Hell S W (1999) Subdiffraction resolution in far-field fluorescence microscopy. *Opt. Lett.* 24: 954–956.
6. Rust M J, Bates M, Zhuang X (2006) Sub-diffraction-limit imaging by stochastic optical reconstruction microscopy (STORM). *Nat. Methods* 3: 793–795.
7. Betzig E, Patterson G H, Sougrat R, Lindwasser O W, Olenych S, Bonifacino J S, Davidson M W, Lippincott-Schwartz J, Hess H F (2006) Imaging intracellular fluorescent proteins at nanometer resolution. *Science* 313: 1642–1645.
8. Dertinger T, Colyer R, Iyer G, Weiss S, Enderlein J (2009) Fast, background-free, 3D super-resolution optical fluctuation imaging (SOFI). *Proc. Natl Acad. Sci. USA* 106: 22287–22292.
9. Fujita K, Kobayashi M, Kawano S, Yamanaka M, Kawata S (2007) High-resolution confocal microscopy by saturated excitation of fluorescence. *Phys. Rev. Lett.* 99: 228105.
10. Yamanaka M, Saito K, Smith N I, Kawata S, Nagai T, Fujita K (2014) Saturated excitation of fluorescent proteins for subdiffraction-limited imaging of living cells in three dimensions. *Interface Focus* 3: 20130007.
11. Gustafsson M G (1999) Extended resolution fluorescence microscopy. *Curr. Opin. Struct. Biol.* 9: 627–634.
12. Gustafsson M G (2000) Surpassing the lateral resolution limit by a factor of two using structured illumination microscopy. *J. Microsc.* 198: 82–87.
13. Gustafsson M G, Shao L, Carlton P M, Wang C J, Golubovskaya I N, Cande W Z, Agard D A, Sedat J W (2008) Three-dimensional resolution doubling in wide-field fluorescence microscopy by structured illumination. *Biophys. J.* 94: 4957–4970.
14. Schermelleh L, Heintzmann R, Leonhardt H (2010) A guide to super-resolution fluorescence microscopy. *J. Cell Biol.* 190: 165–175.
15. Cox S (2015) Super-resolution imaging in live cells. *Dev. Biol.* 401: 175–181.
16. Schermelleh L, Carlton P M, Haase S, Shao L, Winoto L, Kner P, Burke B, Cardoso M C, Agard D A, Gustafsson M G, Leonhardt H, Sedat J W (2008) Subdiffraction multicolor imaging of the nuclear periphery with 3D structured illumination microscopy. *Science* 320: 1332–1336.
17. Strauss M P, Liew A T, Turnbull L, Whitchurch C B, Monahan L G, Harry E J (2012) 3D-SIM super resolution microscopy reveals a bead-like arrangement for FtsZ and the division machinery: implications for triggering cytokinesis. *PLoS Biol.* 10: e1001389.
18. Turnbull L, Strauss M P, Liew A T, Monahan L G, Whitchurch C B, Harry E J (2014) Super-resolution imaging of the cytokinetic Z ring in live bacteria using fast 3D-structured illumination microscopy (f3D-SIM). *J. Vis. Exp.* 29: e51469.
19. Wicker K, Mandula O, Best G, Fiolka R, Heintzmann R (2013) Phase optimisation for structured illumination microscopy. *Optics Express* 21: 2032–2049.
20. Wei F, Lu D, Shen H, Wan W, Ponsetto J L, Huang E, Liu Z (2014) Wide field super-resolution surface imaging through plasmonic structured illumination microscopy. *Nano Lett.* 14: 4634–4639.
21. Ponsetto J L, Wei F F, Liu Z W (2014) Localized plasmon assisted structured illumination microscopy for wide-field high-speed dispersion-independent super resolution imaging. *Nanoscale* 6: 5807–5812.
22. Park J H, Lee S W, Lee E S, Lee J Y (2014) A method for super-resolved CARS microscopy with structured illumination in two dimensions. *Optics Express* 22: 9854–9870.
23. Kner P, Chhun B B, Griffis E R, Winoto L, Gustafsson M G (2009) Super-resolution video microscopy of live cells by structured illumination. *Nat. Methods* 6: 339–342.
24. Shao L, Kner P, Rego E H, Gustafsson M G (2011) Super-resolution 3D microscopy of live whole cells using structured illumination. *Nat. Methods* 8: 1044–1046.
25. Gustafsson M G (2005) Nonlinear structured-illumination microscopy: wide-field fluorescence imaging with theoretically unlimited resolution. *Proc. Natl Acad. Sci. USA* 102: 13081–13086.
26. Rego E H, Shao L, Macklin J J, Winoto L, Johansson G A, Kamps-Hughes N, Davidson M W, Gustafsson M G (2012) Non-linear structured-illumination microscopy with a photoswitchable protein reveals cellular structures at 50-nm resolution. *Proc. Natl Acad. Sci. USA* 109: E135–E143.
27. Müller C B, Enderlein J (2010) Image scanning microscopy. *Phys. Rev. Lett.* 104: 198101.

28. York A G, Parekh S H, Dalle Nogare D, Fischer R S, Temprine K, Mione M, Chitnis A B, Combs C A, Shroff H (2012) Resolution doubling in live, multicellular organisms via multifocal structured illumination microscopy. *Nat. Methods* 9: 749–754.
29. Schulz O, Pieper C, Clever M, Pfaff J, Ruhlandt A, Kehlenbach R H, Wouters F S, Grosshans J, Bunt G, Enderlein J (2013) Resolution doubling in fluorescence microscopy with confocal spinning-disk image scanning microscopy. *Proc. Natl Acad. Sci. USA* 110: 21000–21005.
30. York A G, Chandris P, Nogare D D, Head J, Wawrzusin P, Fischer R S, Chitnis A, Shroff H (2013) Instant super-resolution imaging in live cells and embryos via analog image processing. *Nat. Methods* 10: 1122–1126.
31. Gao L, Shao L, Higgins C D, Poulton J S, Peifer M, Davidson M W, Wu X, Goldstein B, Betzig E (2012) Noninvasive imaging beyond the diffraction limit of 3D dynamics in thickly fluorescent specimens. *Cell* 151: 1370–1385.
32. Chen B C, Legant W R, Wang K, Shao L, Milkie D E, Davidson M W, Janetopoulos C, Wu X S, Hammer J A III, Liu Z, English B P, Mimori-Kiyosue Y, Romero D P, Ritter A T, Lippincott-Schwartz J, Fritz-Laylin L, Mullins R D, Mitchell D M, Bembenek J N, Reymann A C, Bohme R, Grill S W, Wang J T, Seydoux G, Tulu U S, Kiehart D P, Betzig E (2014) Lattice light-sheet microscopy: imaging molecules to embryos at high spatiotemporal resolution. *Science* 346: 1257998.
33. Ando R, Mizuno H, Miyawaki A (2004) Regulated fast nucleocytoplasmic shuttling observed by reversible protein highlighting. *Science* 306: 1370–1373.
34. Habuchi S, Ando R, Dedecker P, Verheijen W, Mizuno H, Miyawaki A, Hofkens J (2005) Reversible single-molecule photo-switching in the GFP-like fluorescent protein Dronpa. *Proc. Natl Acad. Sci. USA* 102: 9511–9516.
35. Habuchi S, Dedecker P, Hotta J, Flors C, Ando R, Mizuno H, Miyawaki A, Hofkens J (2006) Photo-induced protonation/deprotonation in the GFP-like fluorescent protein Dronpa: mechanism responsible for the reversible photoswitching. *Photochem. Photobiol. Sci.* 5: 567–576.
36. Schwentker M A, Bock H, Hofmann M, Jakobs S, Bewersdorf J, Eggeling C, Hell S W (2007) Wide-field subdiffraction RESOLFT microscopy using fluorescent protein photoswitching. *Microsc. Res. Tech.* 70: 269–280.
37. Shao L, Isaac B, Uzawa S, Agard D A, Sedat J W, Gustafsson M G (2008) ISS: wide-field light microscopy with 100-nm-scale resolution in three dimensions. *Biophys. J.* 94: 4971–4983.
38. Ingaramo M, York A G, Wawrzusin P, Milberg O, Hong A, Weigert R, Shroff H, Patterson G H (2014) Two-photon excitation improves multifocal structured illumination microscopy in thick scattering tissue. *Proc. Natl Acad. Sci. USA* 111: 5254–5259.
39. Winter P W, York A G, Nogare D D, Ingaramo M, Christensen R, Chitnis A, Patterson G H, Shroff H (2014) Two-photon instant structured illumination microscopy improves the depth penetration of super-resolution imaging in thick scattering samples. *Optica* 1: 181–191.
40. Huisken J, Swoger J, Del Bene F, Wittbrodt J, Stelzer E H (2004) Optical sectioning deep inside live embryos by selective plane illumination microscopy. *Science* 305: 1007–1009.
41. Keller P J, Schmidt A D, Wittbrodt J, Stelzer E H (2008) Reconstruction of zebrafish early embryonic development by scanned light sheet microscopy. *Science* 322: 1065–1069.
42. Gao L, Shao L, Chen B C, Betzig E (2014) 3D live fluorescence imaging of cellular dynamics using Bessel beam plane illumination microscopy. *Nat. Protoc.* 9: 1083–1101.
43. Lin Y, Seka W, Eberly J H, Huang H, Brown D L (1992) Experimental investigation of Bessel beam characteristics. *Appl. Opt.* 31: 2708–2713.
44. Planchon T A, Gao L, Milkie D E, Davidson M W, Galbraith J A, Galbraith C G, Betzig E (2011) Rapid three-dimensional isotropic imaging of living cells using Bessel beam plane illumination. *Nat. Methods* 8: 417–423.
45. Arigovindan M, Sedat J W, Agard D A (2012) Effect of depth dependent spherical aberrations in 3D structured illumination microscopy. *Optics Express* 20: 6527–6541.
46. Babcock H W (1990) Adaptive optics revisited. *Science* 249: 253–257.
47. Milkie D E, Betzig E, Ji N (2011) Pupil-segmentation-based adaptive optical microscopy with full-pupil illumination. *Opt. Lett.* 36: 4206–4208.
48. Ji N, Milkie D E, Betzig E (2010) Adaptive optics via pupil segmentation for high-resolution imaging in biological tissues. *Nat. Methods* 7: 141–147.
49. Wang K, Milkie D E, Saxena A, Engerer P, Misgeld T, Bronner M E, Mumm J, Betzig E (2014) Rapid adaptive optical recovery of optimal resolution over large volumes. *Nat. Methods* 11: 625–628.
50. Boulanger J, Kervrann C, Bouthemy P, Elbau P, Sibarita J B, Salamero J (2010) Patch-based nonlocal functional for denoising fluorescence microscopy image sequences. *IEEE Trans. Med. Imaging* 29: 442–454.
51. Arigovindan M, Fung J C, Elnatan D, Mennella V, Chan Y H, Pollard M, Branlund E, Sedat J W, Agard D A (2013) High-resolution restoration of 3D structures from widefield images with extreme low signal-to-noise-ratio. *Proc. Natl Acad. Sci. USA* 110: 17344–17349.
52. Matsuda A, Shao L, Boulanger J, Kervrann C, Carlton P M, Kner P, Agard D, Sedat J W (2010) Condensed mitotic chromosome structure at nanometer resolution using PALM and EGFP-histones. *PLoS One* 5: e12768.
53. Carlton P M, Boulanger J, Kervrann C, Sibarita J B, Salamero J, Gordon-Messer S, Bressan D, Haber J E, Haase S, Shao L, Winoto L, Matsuda A, Kner P, Uzawa S, Gustafsson M, Kam Z, Agard D A, Sedat J W (2010) Fast live simultaneous multiwavelength four-dimensional optical microscopy. *Proc. Natl Acad. Sci. USA* 107: 16016–16022.
54. Chu K, McMillan P J, Smith Z J, Yin J, Atkins J, Goodwin P, Wachsmann-Hogiu S, Lane S (2014) Image reconstruction for structured-illumination microscopy with low signal level. *Optics Express* 22: 8687–8702.
55. Goldstein T, Osher S (2009) The Split Bregman method for L1-regularized problems. *SIAM J. Imaging Sci.* 2: 323–343.
56. Setzer S, Steidl G, Teuber T (2010) Deblurring Poissonian images by split Bregman techniques. *J. Vis. Commun. Image R* 21: 193–199.
57. Wang Y L, Yang J F, Yin W T, Zhang Y (2008) A new alternating minimization algorithm for total variation image reconstruction. *SIAM J. Imaging Sci.* 1: 248–272.
58. Mudry E, Belkebir K, Girard J, Savatier J, Le Moal E, Nicoletti C, Allain M, Sentenac A (2012) Structured illumination microscopy using unknown speckle patterns. *Nat. Photon.* 6: 312–315.